

Transport theory in the normal state of high- T_c superconductors

Andrew Das Arulsamy^{1,2}

¹ Condensed Matter Group, No. 22, Jln Melur 14, Tmn Melur, Ampang, Selangor DE, Malaysia

² Department of Physics, National University of Singapore, 2 Science Drive 3, Singapore 117542, Singapore

(Dated: March 22, 2022)

Transport mechanism in the normal state of high- T_c superconductors is described using the well known Fermi-Dirac statistics in which an additional restrictive constraint is introduced so as to capture the variation of resistivity with temperature and doping. The additional restrictive condition is the ionization energy that will eventually determine the properties of charge carriers' in the normal state of high- T_c superconductors. The magnitude and the variation of charge carriers concentration and resistivities (polycrystalline, c -axis and ab -planes) with temperature and doping are very well described by the ionization energy based Fermi-Dirac statistics. However, these transport models are not appropriate for cuprates below the characteristics (T^*) and critical temperatures (T_c), metals with free electrons and strong electron-phonon scattering. Ionization energy is found to be an essential parameter to accurately predict variations of resistivity's magnitude with doping, charge carriers' concentrations, scattering rate constants as well as the effective mass. Apart from that, iFDS based resistivity models provide the comprehensive information on crossover-temperature (metallic \rightarrow insulating transition temperature) in the normal state of high- T_c superconductors.

PACS numbers: 71.10.Ay, 74.72.Bk, 72.60.+g, 74.72.-h

I. INTRODUCTION

Superconductivity has been around for almost a century since its discovery in 1911 by Kamerlingh-Onnes [1]. Subsequent discovery on Copper-oxide (Cu-O₂) materials by Bednorz and Muller [2] in 1986 literally questions the applicability of the Nobel prize winning Bardeen-Cooper-Schrieffer (BCS) theory [3] in cuprates. This terrible yet exciting scenario have had led to numerous theoretical proposals and experimental endeavours due to the fact that the transport properties of Cu-O₂ based ceramics are overwhelmingly mystifying. Apart from cuprates, superconductivity seems to occur in almost all type of materials namely, organic Bechgaard salts [4, 5], ferromagnetic [6] ZrZn₂, metallic Magnesium diboride [7], Buckminsterfullerenes [8], Carbon-nanotubes [9] and unbelievably even in DNA [10]. It seems that superconductivity could be one of the fundamental properties of nature that has been elusive prior to Bednorz's discovery. Cuprates and its potential applications were also extensively publicized to the extent where it initiated the superconductivity-renaissance, which was between late 80s and early 90s due to exceptional increase of T_c from about 20 K to 90 K within months. In those days before 1986, reports on superconductivity were revolved around simple metals, metallic alloys and some organic salts. Perhaps due to bad omen, say brought about by the *black* schrodinger cat, scientists have had a hard time to find the correct mechanism for conventional superconductors, which nearly took them 50 years to arrive at BCS theory in 1957. Hopefully history will not repeat itself for the superconducting cuprates that further perplex scientists with its puzzling phenomena. Cuprates, the unique oxide has many *faces* depending upon temperature and doping unlike other known superconductors and electronic materials reported thus far. One of the *face* is of course, superconducting region but there are more than meets the eye such as antiferromagnetic fluctuations, pseudogap, Fermi liquid and non-Fermi liquid as one dopes the cuprates or varies the temperature. As a matter of fact, there have been sufficient amount of experimental results on cuprates that could somehow pin-point the proper ingredients for at least to understand the normal state transport properties of high- T_c superconductors to a certain reasonable extent. Anisotropic phenomena on the normal state resistivity ($\rho(T)$) curves such as the existence of metallic-like conduction, semiconducting property below a certain crossover-temperature ($T_{crossover}$) and incompatibility of $T_{crossover}$ in c -axis with characteristic temperature (T^*) in ab -plane [11, 12] point towards that $T_{crossover}$ in $\rho_c(T)$ could be a different entity from T^* in $\rho_{ab}(T)$. Therefore, it is possible to work-out the details of transport properties in c -axis in accordance with ionization energy based Fermi-Dirac statistics (iFDS) in which the charge carriers is further confined with an additional parameter known as the ionization energy (E_I). In the procedure of deriving iFDS, a somewhat different distribution functions for holes and electrons are also obtained that further justifies the inappropriateness of iFDS for systems consist of free electrons and also for systems which are influenced by strong electron-phonon scattering or both [13, 14]. It is a well established fact that the transport dimensionality in the normal state of high- T_c superconductors is 2-dimensional (2D). As such, comprehensive derivation of iFDS will be carried-out to model the 2D equations of charge carriers' concentrations ($\sqrt{np}(T, E_I)$ and $n(T, E_I)$) and resistivities ($\rho_{poly}(T, E_I)$ and $\rho_c(T, E_I)$) as a function of temperature (T) in the vicinity of electric field that will eventually enable one to enumerate $\sqrt{np}(T, E_I)$, $n(T, E_I)$, $\rho_{poly}(T, E_I)$ and $\rho_c(T, E_I)$. Gapless nature of charge carriers in ab -planes as a consequence of the experimental results by Basov *et al.* [15] is due to an interesting discrepancy between ab -plane

and c -axis in term of superfluid density (ρ_s) and spectral weights in the normal (N_n) and superconducting states (N_s). In c -axis, $\rho_s > N_n - N_s$ while $\rho_s = N_n - N_s$ in ab -plane, which signifies a gapless behavior of charge carriers in ab -planes [16]. This result will also be incorporated into $\rho_{poly}(T, E_I)$ to obtain $\rho_{ab}(T)$. Previously, Anderson and Zou [17] proposed an empirical resistivity equation given by

$$\rho = \frac{A}{T} + BT, \quad (1)$$

for both ab -plane and c -axis. Equation (1) simply suggests that there are two types of competing T -dependences in the normal state of high- T_c superconductors. It is quite obvious that the coexistence of metallic and semiconducting resistivities in both $\rho_{ab}(T)$ and $\rho_c(T)$ are intriguing. Basically, $\rho_c(T, E_I)$ transition occurring from metallic (normal state) superconductor (MS) to metallic-semiconducting crossover (normal state; without T^*) superconductor (MSS) or vice versa with doping is shown to be predictable with models derived from iFDS. It is to be noted that the significance of T^* on $\rho_{ab}(T)$ is ignored in this work since it is still controversial both in terms of experimental and theoretical approaches [11, 12]. Parallel to this, $\rho_{ab}(T)$ and $R_H^{(ab)}(T)$ involving T^* are yet another critical sub-aspects of the above-mentioned conduction peculiarities that need further studies. A theoretical proposal on these phenomena that consist of electrons, spinons and holons was given in Refs. [11, 12] and references therein. Finally, superconducting samples of both crystalline and polycrystalline reported by various research groups will be employed extensively to accentuate the importance of iFDS in the normal state of 2D high- T_c superconductors.

II. IONIZATION ENERGY BASED FERMI-DIRAC STATISTICS

The conduction electron's distribution can be derived using iFDS with ionization energy as an anomalous constraint. This derivation involves two restrictive conditions: (i) the total number of electrons in a given system is constant and (ii) the total energy of n electrons in that system is also constant. Both conditions are as given below

$$\sum_i^\infty n_i = n, \quad (2)$$

$$\sum_i^\infty E_i n_i = E. \quad (3)$$

However, the condition as given in Eq. (3) must be rewritten as given in Eq. (4) by inserting conditions, $E_{electron} = E_{initialstate} + E_I$ and $E_{hole} = E_{initialstate} - E_I$ appropriately.

$$\sum_i^\infty (E_{initialstate} \pm E_I)_i n_i = E. \quad (4)$$

This is to justify that an electron to occupy a higher state N from initial state M is more probable than from initial state L if condition $E_I(M) < E_I(L)$ at certain T is satisfied. As for a hole to occupy a lower state M from initial state N is more probable than to occupy state L if the same condition above is satisfied. $E_{initialstate}$ (E_{is}) is the energy of a particle in a given system at a certain initial state and ranges from $+\infty$ to 0 for electrons and 0 to $-\infty$ for holes. The importance of this inclusion is that it can be interpreted as a gap that will be described later and also, particularly the E_I can be used to estimate the resistivity transition upon substitution of different valence state ions. Utilizing Eq. (4), one can write the mean number of particles in a certain quantum state s (\bar{n}_s) as

$$\bar{n}_s = \frac{\sum_{n_1, n_2, \dots} n_s \exp[-\lambda[n_1(E_{is} \pm E_I)_1 + n_2(E_{is} \pm E_I)_2 + \dots + n_s(E_{is} \pm E_I)_s + \dots]]}{\sum_{n_1, n_2, \dots} \exp[-\lambda[n_1(E_{is} \pm E_I)_1 + n_2(E_{is} \pm E_I)_2 + \dots + n_s(E_{is} \pm E_I)_s + \dots]]}. \quad (5)$$

Since state s was chosen arbitrarily to calculate the mean number of particles in it thus Eq. (5) has to be algebraically rearranged as given below to ease the following derivation

$$\bar{n}_s = \frac{\sum_{n_s} n_s \exp[-\lambda n_s (E_{is} \pm E_I)_s] \sum_{n_1, n_2, \dots}^{(s)} \exp[-\lambda [n_1 (E_{is} \pm E_I)_1 + n_2 (E_{is} \pm E_I)_2 + \dots]]}{\sum_{n_s} \exp[-\lambda n_s (E_{is} \pm E_I)_s] \sum_{n_1, n_2, \dots}^{(s)} \exp[-\lambda [n_1 (E_{is} \pm E_I)_1 + n_2 (E_{is} \pm E_I)_2 + \dots]]}. \quad (6)$$

Note that the sum, $\sum_{n_1, n_2, \dots}^{(s)}$ omits the chosen state, s . Subsequently, the partition function that represents $\sum_{n_1, n_2, \dots}^{(s)}$ can be written as

$$Z_s(n) = \sum_{n_1, n_2, \dots}^{(s)} \exp[-\lambda [n_1 (E_{is} \pm E_I)_1 + n_2 (E_{is} \pm E_I)_2 + \dots]]. \quad (7)$$

Fermi-Dirac statistics, including iFDS also need to satisfy Pauli's exclusion principle apart from the restrictive conditions given in Eqs. (2) and (4) in which, Pauli's principle requires that one needs to sum over $n_s = 0$ and 1. This implies that each state can only accomodate one particle. In doing so, one arrives at Eq. (8) from Eqs. (6) and (7).

$$\begin{aligned} \bar{n}_s &= \frac{0 + \exp[-\lambda n_s (E_{is} \pm E_I)_s] Z_s(n-1)}{Z_s(n) + \exp[-\lambda n_s (E_{is} \pm E_I)_s] Z_s(n-1)} \\ &= \frac{1}{\frac{Z_s(n)}{Z_s(n-1)} \exp[\lambda n_s (E_{is} \pm E_I)_s] + 1}. \end{aligned} \quad (8)$$

Further simplification of Eq. (8) can be performed using the relation (assuming $n \gg 1$)

$$\begin{aligned} \ln Z_s(n-1) &= \ln Z_s(n) - \frac{\partial \ln Z_s}{\partial n}, \\ Z_s(n-1) &= Z_s(n) \exp \left[-\frac{\partial \ln Z_s}{\partial n} \right]. \end{aligned} \quad (9)$$

Taking $\partial \ln Z_s / \partial n = \mu_s = \mu$ as a consequence of large n and substituting it into Eq. (8) will lead one to write

$$\bar{n}_s = \frac{1}{\exp[\mu + \lambda (E_{is} \pm E_I)_s] + 1}. \quad (10)$$

Equation (10) is the ionization energy based Fermi-Dirac statistics and the procedure for deriving it, is identical to standard Fermi-Dirac statistics that is given in Ref. [18].

III. RESISTIVITY MODELS

The probability functions for electrons and holes are derived from Eq. (10) after further considering $\exp[\mu + \lambda(E \pm E_I)] \gg 1$ which are given in Eqs. (11) and (12) respectively [16]

$$f_e(E, E_I) = \exp[-\mu - \lambda(E + E_I)], \quad (11)$$

$$f_h(E, E_I) = \exp[\mu + \lambda(E - E_I)]. \quad (12)$$

The parameters μ and λ are the normalization constants that will be derived shortly from Eqs. (2) and (4) respectively. In the standard FDS, the respective Eqs. (11) and (12) are simply given by

$$f_e(E) = \exp[-\mu - \lambda E], \quad (13)$$

$$f_h(E) = \exp [\mu + \lambda E]. \quad (14)$$

The 2D density of states' (DOS) derivative can be shown to be

$$\frac{dN}{d\mathbf{k}} = \frac{L^2 \mathbf{k}}{2\pi}. \quad (15)$$

Subsequently, the restrictive condition as given in Eq. (2) can be rewritten for both electrons and holes respectively by employing the above-stated 2D $dN/d\mathbf{k}$ as

$$n = \frac{L^2}{2\pi} e^{-\mu - \lambda E_I} \int_0^\infty \mathbf{k} \exp \left(-\lambda \frac{\hbar^2 \mathbf{k}^2}{2m} \right) d\mathbf{k}, \quad (16)$$

$$p = \frac{L^2}{2\pi} e^{\mu - \lambda E_I} \int_{-\infty}^0 \mathbf{k} \exp \left(\lambda \frac{\hbar^2 \mathbf{k}^2}{2m} \right) d\mathbf{k}. \quad (17)$$

Note here that E is substituted with $\hbar^2 \mathbf{k}^2 / 2m$. m is the mass of the charge carriers while n and p are the respective concentrations of electrons and holes. L^2 denotes area in \mathbf{k} -space and $\hbar = h/2\pi$, h is the Planck constant. The respective solutions of Eqs. (16) and (17) are given below

$$e^{\mu + \lambda E_I} = \frac{mL^2}{2n\pi\lambda\hbar^2}, \quad (18)$$

$$e^{\mu - \lambda E_I} = \frac{2p\pi\lambda\hbar^2}{mL^2}, \quad (19)$$

The above-stated solutions were obtained via integral

$$\int_0^\infty \mathbf{x}^{2n+1} \exp(-a\mathbf{x}^2) d\mathbf{x} = \frac{n!}{2a^{n+1}}.$$

Equations (18) and (19) respectively imply that [14]

$$\mu_e(iFDS) = \mu_e + \lambda E_I, \quad (20)$$

$$\mu_h(iFDS) = \mu_h - \lambda E_I. \quad (21)$$

On the other hand, using Eq. (4), one can obtain

$$\begin{aligned} E &= \frac{L^2 \hbar^2}{4m\pi} e^{-\mu - \lambda E_I} \int_0^\infty \mathbf{k}^3 \exp \left(\frac{-\lambda \hbar^2 \mathbf{k}^2}{2m} \right) d\mathbf{k} \\ &= \frac{m}{2\pi} \left(\frac{L}{\lambda \hbar} \right)^2 e^{-\mu - \lambda E_I}. \end{aligned} \quad (22)$$

Equation (22) after appropriate substitution with Eq. (18) is compared with the energy of a 2D ideal gas given below

$$E = nk_B T. \quad (23)$$

Quantitative comparison will eventually leads to $\lambda_{iFDS} = \lambda_{FDS} = 1/k_B T$ where k_B is the Boltzmann constant. Actually, equation (23) can be derived trivially with the procedure given in Refs. [18, 19]. Identical λ between FDS and iFDS has been somewhat anticipated and is not unusual either. Nevertheless, Eqs. (20) and (21) will have enormous consequences on the properties of charge carriers as will be pointed out in the following paragraphs.

The distribution function for electrons and holes can be written explicitly by first denoting $\mu = -E_F$ (Fermi level), $\lambda = 1/k_B T$ and substituting these into Eqs. (11) and (12) will lead one to write

$$f_e(E, E_I) = \exp \left[\frac{E_F - E_I - E}{k_B T} \right]. \quad (24)$$

$$f_h(E, E_I) = \exp \left[\frac{E - E_I - E_F}{k_B T} \right]. \quad (25)$$

It is worth noting that, $-E_I$ in Eq. (25) for holes is a natural consequence of Dirac's theory of antiparticle interpretations [20]. Physically, E_I is due to electron-ion attraction or Coulombic in nature that has to be contrasted with band gap, E_g which arises from energy band splitting. General equations to compute charge carriers' concentrations are as listed below

$$n = \int_0^\infty f_e(E, E_I) N_e(E) dE. \quad (26)$$

$$p = \int_{-\infty}^0 f_h(E, E_I) N_h(E) dE. \quad (27)$$

$N_e(E)$ and $N_h(E)$ are the 2D DOS for electrons and holes respectively. It is now convenient to obtain the geometric-mean concentrations of electrons and holes in the normal state of 2D polycrystalline high- T_c superconductors as [16]

$$\sqrt{np}(T, E_I) = \frac{k_B T}{\pi \hbar^2} (m_e^* m_h^*)^{1/2} \exp \left[\frac{-E_I}{k_B T} \right], \quad (28)$$

Here, $n \approx p$ is assumed to avoid E_F and the 2D DOS is given by

$$N_{e,h}(2D) = \frac{m_{e,h}^*}{\pi \hbar^2}. \quad (29)$$

Note here that $N_{e,h}(2D)$ is independent of E and $m_{e,h}^*$ is the effective mass of either electrons or holes. In order to calculate $\rho_c(T, E_I)$, n needs to be determined first that is given by (from Eq. (26))

$$n(T, E_I) = \frac{m_e^* k_B T}{\pi \hbar^2} \exp \left[\frac{E_F - E_I}{k_B T} \right]. \quad (30)$$

The 2D resistivity models for polycrystals and in c -axis can be derived from an elementary resistivity equation,

$$\rho = \frac{m^*}{ne^2 \tau}. \quad (31)$$

Substituting, $1/\tau = AT^2$ as a consequence of electron-electron interactions and Eq. (28) for n into Eq. (31) gives [16]

$$\rho_{poly}(T, E_I) = \frac{A_2 \pi \hbar^2}{e^2 k_B} T \exp \left[\frac{E_I}{k_B T} \right], \quad (32)$$

Similarly, $\rho_c(T, E_I)$ can be shown to be [13]

$$\rho_c(T, E_I) = \frac{A_2 \pi \hbar^2}{e^2 k_B} T \exp \left[\frac{E_I - E_F}{k_B T} \right], \quad (33)$$

Note that A_2 is a 2D T -independent scattering rate constant in the absence of magnetic field and e is the charge of an electron. Furthermore, one can recall the characteristics of Eq. (1) which has been captured by Eqs. (32) and (33) where both equations also contain two competing T -dependences though in a different proportionality. One can also surmise that for 2D systems, $k_B T_{crossover} = E_I$ for $\rho_{poly}(T)$ and $k_B T_{crossover} = E_I - E_F$ for $\rho_c(T)$. Now, applying the result of gapless nature of charge carriers in ab -planes into Eq. (32) leaves one with [16]

$$\rho_{ab}(T) = \frac{A_2 \pi \hbar^2}{e^2 k_B} T. \quad (34)$$

The nature of gapless phenomena in ab -planes could be due to change in scattering rate that originates from a different Fermi phase space argument in accordance with nested Fermi liquid theory [21]. Note that Eq. (34) is nothing but a special case that satisfy, $E_I \ll T_c$ inequality. It is stressed that the influence of free electrons and T -dependence of electron-phonon scattering were entirely ignored in the $\rho_{poly}(T, E_I)$ and $\rho_c(T, E_I)$ models as given in Eqs. (32) and (33) respectively. Hence, those models are obviously not suitable for conventional metals. Interestingly, the electrons of a 2D semiconductor with E_g can be further gapped with E_I that will lead one to derive $\sqrt{n p}(T, E_I, E_g)$ and $\rho(T, E_I, E_g)$ respectively as

$$\sqrt{n p}(T, E_I, E_g) = \frac{k_B T}{\pi \hbar^2} (m_e^* m_h^*)^{1/2} \exp \left[\frac{-E_I - \frac{1}{2} E_g}{k_B T} \right]. \quad (35)$$

$$\rho(T, E_I, E_g) = \frac{A_2 \pi \hbar^2}{e^2 k_B} T \exp \left[\frac{E_I + \frac{1}{2} E_g}{k_B T} \right], \quad (36)$$

Consequently, electrons in the conduction band ($E > E_g$) will still be influenced by E_I even though $E_I < E_g$ due to E_I 's Coulombic nature between charge carriers and ions.

IV. DISCUSSION

The effect of Nd^{3+} ($E_I = 1234 \text{ kJmol}^{-1}$) substitution into Sr^{2+} ($E_I = 807 \text{ kJmol}^{-1}$) in superconducting $\text{TiSr}_{2-x}\text{Nd}_x\text{CaCu}_2\text{O}_7$ compound [22] was found to increase the $\rho(T)$ in accordance with E_I . This justifies the need for E_I based analysis on doping as pointed out by iFDS. Applications of iFDS in superconductors are explicitly given in Refs. [11, 12, 13, 16]. Recently, Naqib *et al.* [23] have investigated the electrical properties of $\text{Y}_{1-x}\text{Ca}_x\text{Ba}_2(\text{Cu}_{1-y}\text{Zn}_y)_3\text{O}_{7-d}$ superconducting compounds by varying x , y and d . The transition of normal state $\rho(T)$ with Ca^{2+} ($E_I = 867 \text{ kJmol}^{-1}$) doped into Y^{3+} ($E_I = 1253 \text{ kJmol}^{-1}$) sites is in excellent agreement with Eq. (32) of iFDS. But, Zn^{2+} doping is not appropriate to analyze as a function of iFDS only because this substitution will directly disturb the ab -plane conduction of spinons and holons and also in term of oxygen concentration (d), thus the overall conductivity of $\text{Y}_{1-x}\text{Ca}_x\text{Ba}_2(\text{Cu}_{1-y}\text{Zn}_y)_3\text{O}_{7-d}$ polycrystals will be modified in a not-so-simple way [11, 12]. It is easy however, to extract the relation of normal state $\rho(T)$ between $\text{Y}_{0.9}\text{Ca}_{0.1}\text{Ba}_2\text{Cu}_3\text{O}_{7-d}$ and $\text{Y}_{0.8}\text{Ca}_{0.2}\text{Ba}_2\text{Cu}_3\text{O}_{7-d}$ where the normal state $\rho(T)$ is reduced with Ca^{2+} doping for all d (oxygen pressure), since $\text{Y}^{3+}(E_I = 1253 \text{ kJmol}^{-1}) > \text{Ca}^{2+}(E_I = 867 \text{ kJmol}^{-1})$.

In contrast, Sr^{2+} ($E_I = 807 \text{ kJmol}^{-1}$) substitution into Ba^{2+} ($E_I = 734 \text{ kJmol}^{-1}$) sites have decreased the normal state $\rho(T)$ in $\text{Hg}_{0.85}\text{Re}_{0.15}(\text{Ba}_{1-y}\text{Sr}_y)_2\text{Ca}_2\text{Cu}_3\text{O}_{8-\delta}$ unexpectedly [24]. iFDS suggests that $\rho(T)$ should increase with Sr doping into Ba sites since $\text{Sr}^{2+}(E_I = 807 \text{ kJmol}^{-1}) > \text{Ba}^{2+}(E_I = 734 \text{ kJmol}^{-1})$. This contradicting scenario can be explained since the actual doping concentration determined with EDX showed that the concentrations of other elements namely, Re, Ca and Cu also vary with Sr doping into Ba sites. It is quite non-trivial to verify and prove

these by calculating the relative E_I for Ca^{2+} , Sr^{2+} , Ba^{2+} , Re and $\text{Cu}^{2+,3+}$. For comparison purposes, the valence state of Re and Cu are taken to be $3+$ and $2+$ respectively. Arbitrary values of valence state for Re and Cu will *not* affect this analysis since its valence states are assumed to be constant (in this case) for Sr00 , Sr17 and Sr28 . It is known from Ref. [24] that the concentrations and E_I for Sr00 are Re^{3+} (0.15; 1510 kJmol^{-1}), Ba^{2+} (2.10; 734 kJmol^{-1}), Sr^{2+} (0.00; 807 kJmol^{-1}), Ca^{2+} (2.20; 867 kJmol^{-1}) and Cu^{2+} (3.10; 1352 kJmol^{-1}). For Sr17 , it is given by Re^{3+} (0.15; 1510 kJmol^{-1}), Ba^{2+} (0.84; 734 kJmol^{-1}), Sr^{2+} (0.17; 807 kJmol^{-1}), Ca^{2+} (1.97; 867 kJmol^{-1}) and Cu^{2+} (3.12; 1352 kJmol^{-1}). Finally for Sr28 , Re^{3+} (0.14; 1510 kJmol^{-1}), Ba^{2+} (0.74; 734 kJmol^{-1}), Sr^{2+} (0.28; 807 kJmol^{-1}), Ca^{2+} (1.75; 867 kJmol^{-1}) and Cu^{2+} (3.02; 1352 kJmol^{-1}). Therefore, from this data it is possible to calculate the changes of E_I due to the fluctuations of other non-dopant elements' concentrations with Sr doping into Ba sites. One can show that the relative E_I s are as given below for Sr00 , Sr17 and Sr28 respectively.

$$\begin{aligned} E_I^{(\text{Sr00})} &= [0.15(1510)]_{\text{Re}^{3+}} + [2.10(734)]_{\text{Ba}^{2+}} \\ &\quad + [0.00(807)]_{\text{Sr}^{2+}} + [2.20(867)]_{\text{Ca}^{2+}} \\ &\quad + [3.10(1352)]_{\text{Cu}^{2+}} \\ &= 7640 \text{ kJmol}^{-1}, \end{aligned} \quad (37)$$

$$\begin{aligned} E_I^{(\text{Sr17})} &= [0.15(1510)]_{\text{Re}^{3+}} + [0.84(734)]_{\text{Ba}^{2+}} \\ &\quad + [0.17(807)]_{\text{Sr}^{2+}} + [1.97(867)]_{\text{Ca}^{2+}} \\ &\quad + [3.12(1352)]_{\text{Cu}^{2+}} \\ &= 6680 \text{ kJmol}^{-1}, \end{aligned} \quad (38)$$

$$\begin{aligned} E_I^{(\text{Sr28})} &= [0.14(1510)]_{\text{Re}^{3+}} + [0.74(734)]_{\text{Ba}^{2+}} \\ &\quad + [0.28(807)]_{\text{Sr}^{2+}} + [1.75(867)]_{\text{Ca}^{2+}} \\ &\quad + [3.02(1352)]_{\text{Cu}^{2+}} \\ &= 6369 \text{ kJmol}^{-1}. \end{aligned} \quad (39)$$

Hence, the reduction of $\rho(T)$ with Sr doping is justified from Eqs. (37), (38) and (39), which is due to the concentration's fluctuation of Ca , Re and Cu apart from Ba and Sr . All values of E_I including in Eqs. (37), (38) and (39) were averaged in accordance with

$$E_I[X^{z+}] = \sum_{i=1}^z \frac{E_{Ii}}{z}, \quad (40)$$

and should not be taken literally since those E_I s are not absolute values. The absolute values need to be obtained from Eq. (41) below [14]

$$E_I = \frac{e^2}{8\pi\epsilon\epsilon_0 r_B}. \quad (41)$$

If one of the substituting ion is multivalence, then the valence state of that particular ion can be approximated using Eq. (42) below [16]

$$\frac{\delta}{j} \sum_{i=z+1}^{z+j} E_{Ii} + \frac{1}{z} \sum_{i=1}^z E_{Ii} = \frac{1}{q} \sum_{i=1}^q E_{Ii}. \quad (42)$$

The variations of $\rho(T)$ with doping in polycrystalline samples namely, $(\text{Pr}_{1-x}\text{Gd}_x)_{1.85}\text{Ce}_{0.15}\text{CuO}_4$ and $(\text{Pr}_{1-x}\text{Y}_x)_{1.85}\text{Ce}_{0.15}\text{CuO}_4$ from Meen *et al.* [25], $\text{Pr}_x\text{Gd}_{1-x}\text{Ba}_2\text{Cu}_3\text{O}_{7-\delta}$ from Khosroabadi *et al.* [26] can be explained in a straight-forward manner without even using Eq. (42). Meen *et al.* [25] found that substitutions of Gd^{3+} and Y^{3+} into Pr^{3+} give rise to $\rho(T)$ simply because $E_I(\text{Pr}^{3+} = 1211 \text{ kJmol}^{-1}) < E_I(\text{Gd}^{3+} = 1251 \text{ kJmol}^{-1})$ and $E_I(\text{Pr}^{3+})$

$< E_I(Y^{3+} = 1253 \text{ kJmol}^{-1})$. Similarly, Khosroabadi *et al.* [26] observed decreasing $\rho(T)$ for Pr^{3+} substitution into Gd^{3+} due to former inequality. Further indirect observation was given by Isawa *et al.* [27] for $\text{Ce}_x\text{Pr}_{1-x}\text{La}_2\text{CuO}_{4+\delta}$ polycrystals. However, the valence state of Ce is unknown in that sample therefore one has to employ Eq. (42). The first term, $\frac{\delta}{j} \sum_{i=z+1}^{z+j} E_{Ii}$ in Eq. (42) has $i = z + 1, z + 2, \dots, z + j$ and $j = 1, 2, 3, \dots$. It is solely due to multivalence ion. In this case $\text{Ce}^{3+,4+}$ is substituted into Pr^{3+} sites hence from Eq. (42), the first term is due to Ce^{4+} ion's contribution or caused by reaction of the form $\text{Ce}^{3+} - \text{electron} \rightarrow \text{Ce}^{4+}$ (3547 kJmol^{-1}), hence j is equals to 1 here and δ represents the additional contribution from Ce^{4+} . The second ($i = 1, 2, 3, \dots, z$) and last ($i = 1, 2, 3, \dots, q$) terms respectively are due to reaction of the form $\text{Ce} - 3(\text{electrons}) \rightarrow \text{Ce}^{3+}$ and $\text{Pr} - 3(\text{electrons}) \rightarrow \text{Pr}^{3+}$. Recall that $q = z = 3+$ and $i = 1, 2, 3, \dots$ represent the first, second, third, ... ionization energies while $j = 1, 2, 3, \dots$ represent the fourth, fifth, sixth, ... ionization energies. Therefore, $z + \delta$ gives the minimum valence number for Ce which can be calculated from Eq. (42). Apparently, Ce^{3+} ($E_I = 1178 \text{ kJmol}^{-1}$) substitution into Pr^{3+} ($E_I = 1211 \text{ kJmol}^{-1}$) will lead to a lower $\rho(T)$ as indicated in Ref. [27]. The opposite scenario, increment of $\rho(T)$ with $\text{Ce}^{3+\delta}$ is possible if and only if the valence state of Ce is > 3.010 . This value (3.010) is actually obtained from Eq. (42).

Interestingly, Shi *et al.* [28] have reported substitution effects of $\text{Ru}_{1-x}\text{Sb}_x\text{Sr}_2\text{Gd}_{1.4}\text{Ce}_{0.6}\text{Cu}_2\text{O}_{10-\delta}$ polycrystals on $\rho(T)$. Since $E_I(\text{Sb}^{3+} = 1623 \text{ kJmol}^{-1}) < E_I(\text{Ru}^{3+} = 1692 \text{ kJmol}^{-1})$ then it is quite obvious to predict $\rho(T)$ will be reduced in magnitude with Sb^{3+} content. However, a contradicting scenario have been observed where $\rho(T)$ increases with Sb. As such, Eq. (42) is again useful to estimate the minimum valence state of $\text{Sb}^{3+\delta}$ in order to justify $\rho(T)$ increment with Sb. The minimum valence state of Sb has to be $> 3 + (z + \delta)$ so as to satisfy $\rho(T)$ increment. $z + \delta$ is calculated to be 3.017 or $\text{Sb}^{3.017+}$. Another point worth extracting is that additional annealing (4 days) for $\text{RuSr}_2\text{Gd}_{1.4}\text{Ce}_{0.6}\text{Cu}_2\text{O}_{10-\delta}$ (sample B) does not change E_I significantly whereas the A_2 parameter is reduced dramatically compared to as-prepared sample (A). The assumption that E_I changes insignificantly with annealing is valid since the shape of $\rho(T)$ curves for samples A and B are identical [28]. This phenomenon clearly indicate that long hours of proper heat-treatment improves sample B's quality in terms of grain boundaries, defects [28] and subsequently reduces the magnitude of scattering rates (A_2). Figure 1 indicates calculated plots of $\rho(T, E_I)$ for $\text{Hg}_{0.7}\text{Cr}_{0.3}\text{Sr}_2\text{CuO}_{4+\delta}$ from Ref. [29] and $\text{Gd}_{0.95}\text{Pr}_{0.05}\text{Ba}_2\text{Cu}_3\text{O}_{7-\delta}$ from Ref. [26] while the inset is for $\text{Sr}_{0.9}\text{La}_{0.1}\text{CuO}_2$ from Ref. [30] and $\text{TmBa}_2\text{Cu}_3\text{O}_{6.99}$ from Ref. [31]. Note that the symbols do not represent the experimental data points but simply to enhance contrast between all those calculated curves of different compositions. $\rho(T)$ curves were obtained by fitting experimental data with Eq. (32). Table 1 lists all the fitting parameters namely, T -independent scattering rate constant (A_2), charge carriers concentrations ($\sqrt{n\bar{p}}$), charge gap parameter (E_I) and $d\rho(T)/dT$ in detail above T_c and T^* . $\sqrt{n\bar{p}}$ is estimated by first computing E_I from Eq. (32) and then substitute it into Eq. (28). Furthermore, two values of $\sqrt{n\bar{p}}$ are computed at 300 K, in which one satisfies $m^*/m_o = 1$ while the other takes $m^*/m_o = 50$. m_o is the rest mass of an electron and the fitted values of A_2 are actually equal to $A_2\pi\hbar^2/e^2k_B$. Sulkowski *et al.* [31], have computed charge carriers concentrations from Hall effect measurements for $\text{TmBa}_2\text{Cu}_3\text{O}_{6.99}$ that is in the order of 10^{22} cm^{-3} . This value is comparable with the estimated value from Eq. (28) with $m^*/m_o = 50$, which is $4.7 \times 10^{18} \text{ m}^{-2} = 4.7 \times 10^{22} \text{ cm}^{-3}$. Parallel to this, Eqs. (32) and (28) also enable one to approximate the effective mass of charge carriers. As for single crystals, one may still employ Eq. (32) via the assumption [16]

$$\rho_{poly}(T) = \sqrt{\rho_c(T)\rho_{ab}(T)}. \quad (43)$$

Eq. (43) is assumed to be valid to convert both $\rho_c(T)$ and $\rho_{ab}(T)$ data to $\rho_{poly}(T)$, which will enable one to analyze the effect of A_2 parameter between single crystals and polycrystals. One should not substitute Eqs. (33) and (34) into Eq. (43) because Eq. (34) was derived based on a special case as mentioned previously. Subsequently, the changes on scattering rate (A_2) will be captured. Recently, Lanzara *et al.* [32] have shown quite convincingly via ARPES measurements that the existence of electron-phonon coupling associated with movements of oxygen atoms in $\text{Bi}_2\text{Sr}_2\text{CaCu}_2\text{O}_8$, $\text{Bi}_2\text{Sr}_2\text{Cu}_2\text{O}_6$ and $\text{La}_{2-x}\text{Sr}_x\text{CuO}_4$ should not be neglected entirely. This observation could be due to polarons that is well represented by E_I in iFDS. The important difference between polarons and free electron-phonon scattering is that the latter has a very strong T -dependence while the former increases the effective mass of the charge carriers to some extent. This could be the sole reason for the missing electron-phonon coupling effect on $\rho(T)$ measurements in high- T_c superconducting cuprates thus far. All E_I values were obtained from Ref. [33] and the predictions stated above are only valid for reasonably pure materials without any significant impurity phases and grain boundary effects.

V. CONCLUSIONS

In summary, iFDS is shown to be an appropriate theory in the normal state of high- T_c superconductors. The variations on polycrystalline resistivity with doping were very well explained with one exception, in which the importance

FIG. 1: Computed $\rho(T, E_I)$ curves for $\text{Hg}_{0.7}\text{Cr}_{0.3}\text{Sr}_2\text{CuO}_{4+\delta}$ and $\text{Gd}_{0.95}\text{Pr}_{0.05}\text{Ba}_2\text{Cu}_3\text{O}_{7-\delta}$ from Refs. [29] and [26] respectively. The inset is for $\text{Sr}_{0.9}\text{La}_{0.1}\text{CuO}_2$ and $\text{TmBa}_2\text{Cu}_3\text{O}_{6.99}$ from Refs. [30] and [31] respectively. The curves were determined in accordance with Eq. (32). The symbols were used solely to distinguish curves of different samples and it does not represent experimental data points. Apparently, $T_{\text{crossover}}$ s for all these samples (if any) are $< T_c$ s, as such the metal to semiconductor transition is not observed, which has been anticipated because $E_I < k_B T_c$.

TABLE I: Computed values of the temperature independent scattering rate constant (A_2), charge gap parameter (E_I), resistivity slope ($d\rho(T)/dT$) and the concentration of charge carriers (\sqrt{np}) at 300 K with different effective masses ($m^*/m_o = 1$ and $m^*/m_o = 50$) in the normal state of high- T_c superconducting polycrystals. Note that the magnitudes of E_I are in the range of 2-9 meV and the charge carriers' concentration is determined to be in the order of 10^{18} m^{-2} or 10^{22} cm^{-3} if $m^*/m_o = 50$ is assumed. $d\rho(T)/dT$ is calculated from the experimental $\rho_{\text{poly}}(T)$ linear plots.

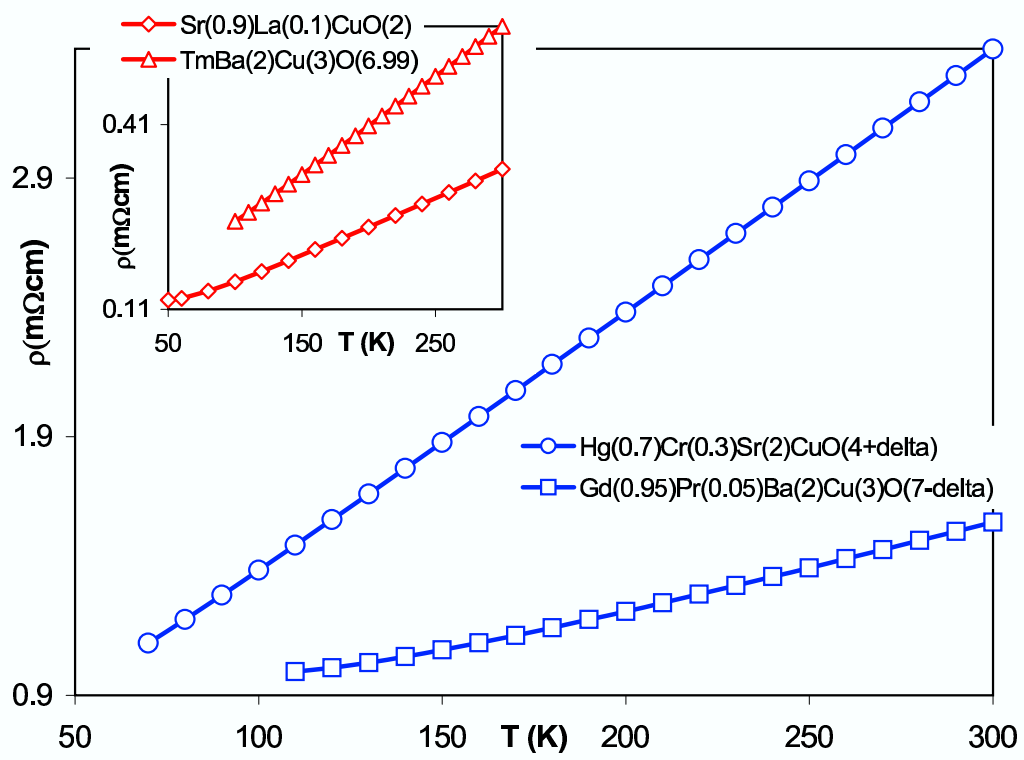
of characteristics temperature was ignored throughout this work partly due to vague understanding on temperature dependence of c -axis and ab -plane scattering rates. It is interesting to note that iFDS is able to predict the resistivity's magnitude with doping via ionization energy as well as enable one to estimate the valence state of substituting ions accurately. Apart from that, the fitting parameters give a reasonable prediction of the charge carriers' effective mass in the vicinity of 10^{-29} kg or 50 times heavier than electron's rest mass. The concentration of this heavy charge carriers is around 10^{22} cm^{-3} whereas light charge carriers' concentration is approximately 10^{20} cm^{-3} when the effective mass is equals to rest mass. The heavier effective mass ($1 < m^*/m_o \leq 50$) somewhat imply the existence of polarons in the normal state of high- T_c superconductors that could mask electron-phonon coupling effect on resistivity versus temperature measurements.

Acknowledgments

ADA would like to thank the National University of Singapore for the financial aid and also to Prof. Feng Yuan Ping for his support. ADA personally thanks Saleh H. Naqib and his group for their kind approval of using their experimental data on cuprates prior to publication as well as Dr Igor Yurin for his helpful comments on Cooperon in Cuprates. The author is grateful and beholden to Arulsamy Innasimuthu, Sebastiammal Innasimuthu, Arokia Das Anthony and Cecily Arokiam, whom are the financiers of private (non-governmental) and not-for-profit Condensed Matter Group (CMG-Ampang), which was founded solely for the advancement of science.

-
- [1] H. Kamerlingh-Onnes, Proc. R. Acad. Amsterdam **13**, 1903 (1911).
 - [2] J. G. Bednorz and K. A. Muller, Z. Phys. B **64**, 189 (1986).
 - [3] J. Bardeen, L. N. Cooper, J. R. Schrieffer, Phys. Rev. **108**, 1175 (1957).
 - [4] D. Jerome, A. Mazaud, M. Ribault, K. Bechgaard, J. Phys. Lett. (Paris) **41**, L95 (1980).
 - [5] K. Bechgaard, K. Carneiro, M. Olsen, F. Rasmussen and C. S. Jacobsen, Phys. Rev. Lett. **46**, 852 (1981).
 - [6] C. Pfeleiderer, M. Uhlarz, S. M. Hayden, R. Vollmer, H. v. Lohneysen, N. R. Bernhoeft, G. G. Lonzarich, Nature **412**, 58 (2001).
 - [7] J. Nagamatsu, N. Nakagawa, T. Muranaka, Y. Zenitani, J. Akimitsu, Nature **410**, 63 (2001).
 - [8] M. L. Cohen, V. H. Crespi, *Theory of Electronic and Superconducting Properties of Fullerenes* (in Buckminsterfullerenes, eds. W. E. Billups, M. A. Ciufolini, VCH Publishers, New York, 1993).
 - [9] P. Sheng, N. Wang, Z.-K. Tang, Science **292**, 2462 (2001).
 - [10] A. Yu. Kasumov, M. Kociak, S. Gueron, B. Reulet, V. T. Volkov, D. V. Klinov, H. Bouchiat, Science **291**, 280 (2001).
 - [11] A. Das Arulsamy, P. C. Ong, M. T. Ong, Physica B **325**, 164 (2003).
 - [12] A. Das Arulsamy, cond-mat/0206293, (<http://arxiv.org>).
 - [13] A. Das Arulsamy, Physica C **356**, 62 (2001).
 - [14] A. Das Arulsamy, cond-mat/0212202, (<http://arxiv.org>).
 - [15] D. N. Basov, S. I. Woods, A. S. Katz, E. J. Singley, R. C. Dynes, M. Xu, D. G. Hinks, C. C. Homes, M. Strongin, Science **283**, 49 (1999).
 - [16] A. Das Arulsamy, Phys. Lett. A **300**, 691 (2002).
 - [17] P. W. Anderson, Z. Zou, Phys. Rev. Lett. **60**, 132 (1988).
 - [18] F. Reif, *Fundamentals of statistical and thermal physics*, (McGraw-Hill, Inc., Tokyo, 1981).
 - [19] D. Halliday, R. Resnick, *Physics: Parts 1 and 2*, (John Wiley and Sons, 3rd edn., New York, 1978).
 - [20] J. J. Sakurai, *Advanced quantum mechanics*, (Addison-Wesley, Inc., USA, 1967).

- [21] A. Virosztek, J. Ruvalds, Phys. Rev. B **45**, 347 (1992).
- [22] R. Abd-Shukor, A. Das Arulsamy, J. Phys. D **33**, 836 (2000).
- [23] S. H. Naqib, J. R. Cooper, J. L. Tallon, C. Panagopoulus, Physica C **387**, 365 (2003).
- [24] A. J. Batista-Leyva, M. T. D. Orlando, L. Rivero, R. Cobas, E. Altshuler, Physica C **383**, 365 (2003).
- [25] T. H. Meen, H. D. Yang, W. J. Huang, Y. C. Chen, W. H. Lee, J. H. Shieh, H. C. Ku, Physica C **260**, 117 (1996).
- [26] H. Khosroabadi, V. Daadmehr, M. Akhavan, Physica C **384**, 169 (2003).
- [27] K. Isawa, M. Nagano, M. Fujita, K. Yamada, Physica C **378-381**, 142 (2002).
- [28] L. Shi, G. Li, X. D. Zhang, S. J. Feng, X. -G. Li, Physica C **383**, 450 (2003).
- [29] E. Kandyel, M. A. Sekina, J. Phys. Chem. Solids **63**, 1815 (2002).
- [30] S. Karimoto, K. Ueda, M. Naito, T. Imai, Physica C **378-381**, 127 (2002).
- [31] C. Sulkowski, D. Wlosewicz, M. Matusiak, T. Plackowski, A. Sikora, R. Horyn, Physica C **387**, 187 (2003).
- [32] A. Lanzara, P. B. Bogdanov, X. J. Zhou, S. A. Keller, D. L. Feng, E. D. Lu, T. Yoshida, H. Eisaki, A. Fujimori, K. Kishio, J. -I. Shimoyama, T. Noda, S. Uchida, Z. Hussain, Z. -X. Shen, Nature **412**, 510 (2001).
- [33] M. J. Winter, (<http://www.webelements.com>).



A. Das Arulsamy
Figure 1

A. Das Arulsamy
Table 1

Samples, [Ref.]	A_2	E_I [K]	E_I [meV]	$\sqrt{np} \times 10^{16}$ [m ⁻²] 300 K m*/m ₀ = 1	$\sqrt{np} \times 10^{18}$ [m ⁻²] 300 K m*/m ₀ = 50	dρ(T) / dT [μΩ-cmK ⁻¹]
TmBa ₂ Cu ₃ O _{6.99} [31]	1.6455×10^{-3}	43.1	3.71	9.354	4.677	1.60
Sr _{0.9} La _{0.1} CuO ₂ [30]	9.6000×10^{-4}	47.8	4.20	9.208	4.604	-
Hg _{0.7} Cr _{0.3} Sr ₂ CuO _{4+δ} [29]	1.0250×10^{-2}	30.0	2.59	9.771	4.886	1.00
Gd _{0.95} Pr _{0.05} Ba ₂ Cu ₃ O _{7-δ} [26]	3.8200×10^{-3}	94.4	8.13	7.884	3.942	3.10
YBa ₂ Cu ₃ O ₇ Sample B, [16]	1.1458×10^{-8}	89.2	7.69	8.022	4.011	-
YBa ₂ Cu ₃ O ₇ Sample C, [16]	1.1268×10^{-8}	94.0	8.11	7.895	3.948	-
GaSr ₂ (Y _{0.6} Ca _{0.4})Cu ₂ O ₇ , [16]	1.3002×10^{-5}	69.3	5.98	8.572	4.286	~0
YSrBaCu ₃ O ₇ Sample [O], [16]	1.1712×10^{-6}	53.5	4.61	9.036	4.518	1.10
Y _{0.8} Pr _{0.2} SrBaCu ₃ O ₇ Sample [O], [16]	1.8589×10^{-6}	76.6	6.61	8.366	4.183	1.60
YBa ₂ Cu ₃ O _x , [16]	5.5747×10^{-6}	95.6	8.25	7.853	3.926	4.25
YBa ₂ Cu ₃ O _{7-x} Sample A, [16]	6.3767×10^{-6}	92.0	7.94	7.948	3.974	5.00
Y(Ba _{0.85} Pb _{0.15}) ₂ Cu ₃ O _{7-x} Sample B, [16]	5.4926×10^{-6}	79.8	6.88	8.278	4.139	4.90
Tl(Sr _{1.6} Sm _{0.4})CaCu ₂ O _{7-x} , [16]	2.8695×10^{-5}	59.5	5.13	8.857	4.430	2.60
Tl(Sr _{1.6} Dy _{0.4})CaCu ₂ O _{7-x} , [16]	2.2192×10^{-5}	66.2	5.71	8.661	4.330	2.00